







Research Article

Hydrothermal Synthesis of Li_2MnO_3 -Stabilized LiMnO_2 as a Cathode Material for Li-Ion Battery

Ngoc Hung Vu ^{1,2}, Van-Duong Dao ^{1,2}, Hong Ha Thi Vu ^{1,2}, Nguyen Van Noi,³
Dinh Trinh Tran ³, Minh Ngoc Ha ³, and Thanh-Dong Pham ³

¹Faculty of Biotechnology, Chemistry and Environmental Engineering, Phenikaa University, Hanoi 10000, Vietnam

²Phenikaa Research and Technology Institute (PRATI), A&A Green Phoenix Group, 167 Hoang Ngan, Hanoi 10000, Vietnam

³Faculty of Chemistry, University of Science, Vietnam National University, 334 Nguyen Trai, Thanh Xuan, Hanoi, Vietnam

Correspondence should be addressed to Ngoc Hung Vu; hung.vungoc@phenikaa-uni.edu.vn

Received 25 May 2021; Accepted 26 June 2021; Published 12 July 2021

Academic Editor: Domenico Acierno

Copyright © 2021 Ngoc Hung Vu et al. This is an open access article distributed under the Creative Commons Attribution License, which permits unrestricted use, distribution, and reproduction in any medium, provided the original work is properly cited.

Herein, we reported the composite structure of LiMnO_2 and Li_2MnO_3 as a low-cost and environmentally benign cathode material. This composite with the main phase of LiMnO_2 (90%) was synthesized by hydrothermal method at 220°C from LiOH and $\text{Mn}(\text{CH}_3\text{COO})_2$ precursors. The obtained nanosized LiMnO_2 - Li_2MnO_3 cathode material exhibits a high capacity of 265 mAh g^{-1} at C/10. The incorporation of Li_2MnO_3 into the LiMnO_2 phase could stabilize the structure, leading to the improved cycle stability of the cathode. The capacity retention of the cathode was 93% after 80 cycles at C/2. Our results facilitate a potential strategy for developing high-performance cathode materials based on the Li-Mn-O system.

1. Introduction

Although lithium-ion batteries (LIBs) have a dominant position as the power source in mobile electronics, they still do not meet the growing demand for these power-consuming devices [1]. In addition, the reduction of product costs, including production costs and treatment costs that affect the environment after disposal, is of considerable concern to manufacturers. Accordingly, the use of inexpensive and environmentally friendly commercial cathode materials such as LiMn_2O_4 and LiFePO_4 takes precedence over LiCoO_2 under these conditions [2, 3]. Compared with Fe-based materials, Mn-based materials have a higher range of working potential and conductivity. Accordingly, there are many other Mn-based materials that are studied such as LiMnO_2 , Li_2MnO_3 , $\text{Li}_4\text{Mn}_5\text{O}_{12}$, and $\text{Li}_4\text{Mn}_2\text{O}_5$ and their composites [4–8]. These materials exhibit superior capacity than available commercial cathode materials and are expected to fulfill the requirement in electric vehicle application. Freire et al. [9] reported that a rock-salt structure of $\text{Li}_4\text{Mn}_2\text{O}_5$ which is synthesized by a mechanochemical synthesis method could deliver a high capacity of 355 mAh g^{-1} . Liu et al. [10] reported

the synthesis of $\text{Li}_4\text{Mn}_5\text{O}_{12}$ at low temperature by solid-state reaction, and the cathode could deliver a high capacity of 212 mAh g^{-1} . Li_2MnO_3 has the highest theoretical capacity among others (485 mAh g^{-1}), and it has been extensively studied in the Li-rich layered oxide system (LLO) as a structural stabilizer and a capacity booster. On the other hand, LiMnO_2 also has high theoretical capacity of 285 mAh g^{-1} . It has a lot of metastable states including orthorhombic (*o*- LiMnO_2 , space group *Pmmn*), monoclinic (*m*- LiMnO_2 , space group *C2/m*), and layered LiMnO_2 (space group *R3m*) with α - NaFeO_2 -like structure. Among these structures, the *o*- LiMnO_2 is the most stable. However, the single phase of Mn-based compounds, such as Li_2MnO_3 , LiMnO_2 , or $\text{Li}_4\text{Mn}_5\text{O}_{12}$, cannot be used as a cathode material for LIBs due to their structural instability. As a way to overcome some of these difficulties, compounds derived from the substitution of Mn by Ni and Co have been studied. The other way is designing a composite structure between them. The LLO, which is $x\text{Li}_2\text{MnO}_3 \cdot (1-x)\text{LiMO}_2$ ($M = \text{Mn, Ni, Co}$), has more than two decades of investigation [11–13]. To promote using standing Mn-based materials, we investigate the stabilization of Li_2MnO_3 for LiMnO_2 as cathode materials for LIBs.

2. Experimental

The integrated structure was synthesized by a hydrothermal method. First, manganese (II) acetate tetrahydrate (4.9 g, Sigma-Aldrich) and lithium hydroxide monohydrate (3.36 g, Sigma-Aldrich) were dissolved in distilled water (40 mL) separately. Then, hydrogen peroxide (H₂O₂, 30% (w/w) in H₂O, 1.6 mL) was added to the Li solution before adding Mn solution slowly. The mixture was mixed with methanol (20 mL) and stirred for 0.5 h. Subsequently, it was located into a Teflon-lined autoclave for the hydrothermal reaction at 220°C for 12 h. Finally, the powder was centrifuged and washed with ethanol and distilled water thoroughly.

The phase of the sample was identified by X-ray diffraction (XRD) measurements using Philips X'Pert with Cu-K α radiation in a range of $10^\circ \leq 2\theta \leq 100^\circ$. The morphology of particles was recorded by scanning electron microscopy (SEM, Nova NanoSEM 450) and high-resolution transmission electron microscopy (HRTEM, JOEL JEM-2100F). The oxidation state of elements was determined by X-ray photon spectroscopy (XPS, K-Alpha+ Thermo Scientific). The chemical composition was analyzed by ICP (Optima 8300 ICP-OES spectrometer).

For cathode fabrication, the active material (70 wt%), Ketjen black (10 wt%), and teflonized acetylene black (binder, 20 wt%) were mixed thoroughly. Then, it was pressed onto a stainless-steel mesh and dried at 120°C under vacuum for 12 h. For coin-cell (2032 coin-type cell) fabrication, the cathode, an electrolyte (1 M LiPF₆ solution in a 1 : 1 mixture of ethylene carbonate and dimethyl carbonate), a separator, and Li metal were assembled in an Ar-filled glovebox. The cell was tested of its electrochemical properties by a Neware Battery Tester between 2.0 and 4.8 V vs. Li⁺/Li.

3. Results and Discussion

3.1. Structural Characterization of Cathode. Figure 1 shows the XRD pattern of the synthesized sample. All peaks can be indexed according to the space group *Pmnm* of the orthorhombic LiMnO₂ structure. There is a slightly weak peak that appears at $\sim 18.3^\circ$, which is assignable to the Li₂MnO₃ phase (space group *C2/m*). This second phase originated from the oxidation decomposition reaction [14]. All peaks are sharp, indicating the high crystallinity of particles. Note that the ratio of LiMnO₂ to Li₂MnO₃ phase can be changed by using an oxidizing agent [15] or controlling the synthesis temperature [16]. The ICP result shows that the ratio of Li : Mn = 1.095 : 1 due to the existence of the Li₂MnO₃ phase. Rietveld refinement is performed using the model shown in Table 1. The main phase is *o*-LiMnO₂ with space group *Pmnm*, and the second phase is Li₂MnO₃ with space group *C2/m*. In the *o*-LiMnO₂ structure, Mn and Li occupy the *2a* Wyckoff site. The oxygen occupies the *2b* Wyckoff site. The oxygen array is distorted from ideal cubic-close packing due to Jahn-Teller effect on Mn³⁺. The structure is built up from independent MnO₆ and LiO₆ octahedra that are arranged in corrugated layers. The Rietveld refinement shows that the degree of substitution of Li/Mn in the octahedra is about

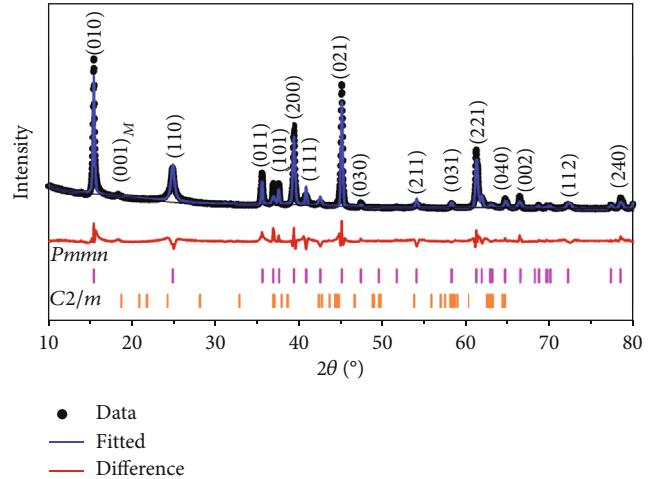


FIGURE 1: XRD pattern of prepared sample indexed against the standard *o*-LiMnO₂ (PDF #35-0749, space group *Pmnm*) and Li₂MnO₃ phase (PDF #84-1634, space group *C2/m*).

TABLE 1: Rietveld refinement and crystal data obtained from the XRD data.

Phase	<i>o</i> -LiMnO ₂	Li ₂ MnO ₃
Space group	<i>Pmnm</i>	<i>C2/m</i>
Phase fraction	90%	10%
Lattice parameter (Å)	$a = 4.5758$	$a = 4.8660$
	$b = 5.7482$	$b = 8.4210$
	$c = 2.8100$	$c = 5.0257$
		$\beta = 108.9202$
Li/Mn substitution	5%	
Fitting quality		R_p (%) = 5.35
		R_{wp} (%) = 8.03
		χ^2 (%) = 10.99

5%. The cation disorder can improve the electrochemical performance of the cathode [17–19]. The lattice parameter of *o*-LiMnO₂ is slightly smaller than that in literature [20]. This might be caused by the effect of the Li₂MnO₃ phase.

SEM and TEM analyses were performed to study the particle's morphology and are shown in Figure 2. Accordingly, the particles have a well-defined shape (Figure 2(a)). The particles are elongated, parallelogram-shaped grains. The particle size ranges from 100 to 400 nm. The *d*-spacing is calculated as 0.588 nm, which corresponds to the (010) plane at $2\theta = 15^\circ$. These results further confirm the predominance of the *o*-LiMnO₂ phase with good crystallinity of the particles.

To examine the oxidation state of Mn in the compound, XPS measurement was carried out and shown in Figure 3. The survey XPS profiles (Figure 3(a)) contain peaks at ~ 641 , 530, 285, and 55 eV, which are allocated for Mn 2p, O 1s, C 1s, and Li 1s, respectively. This indicates the presence of Li, Mn, C, and O in the sample. The presence of C is due to the absorption of CO₂ from the air onto the sample's surface

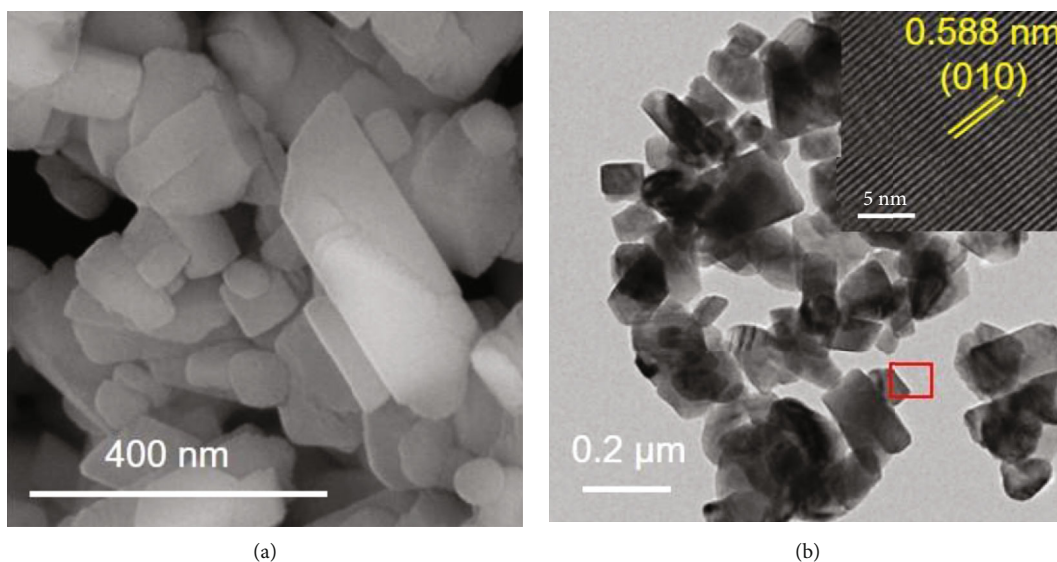


FIGURE 2: (a) SEM and (b) TEM of the sample. Enlarged image of marked region shows lattice fringe.

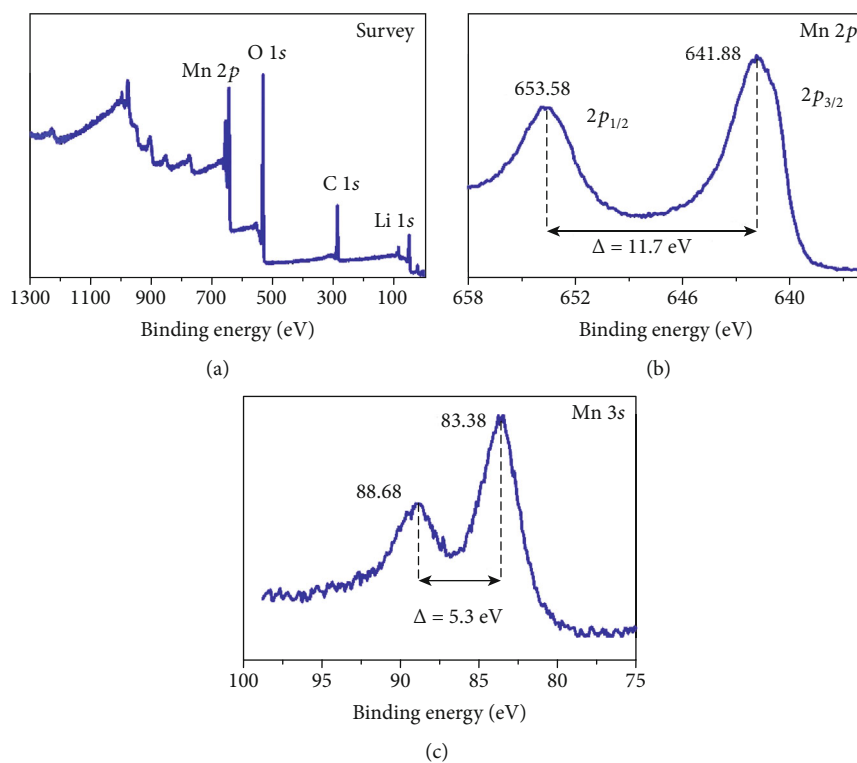


FIGURE 3: XPS spectra of (a) survey, (b) Mn 2p, and (c) Mn 3s of the sample.

[21–23]. Figure 3(b) shows the Mn 2p core-level spectrum, which exhibits two peaks, namely, Mn $2p_{3/2}$ and Mn $2p_{1/2}$. These peaks locate at 641.88 and 653.58 eV, respectively, with the spin-orbital splitting value of 11.7 eV. The binding energy of Mn $2p_{3/2}$ of the sample is in between binding energy of those in Mn_2O_3 (641.6 eV) and MnO_2 (642.6 eV) [24]. This result indicates the coexistence of both Mn^{3+} and Mn^{4+} in the sample. Figure 3(c) shows the Mn 3s spectrum to further evaluate the oxidation state of Mn. The splitting in Mn 3s

spectrum is caused by the coupling of the nonionized 3s electron with 3d valence-band electrons, and its value indicates the oxidation state of Mn. Here, it is 5.3 eV so the oxidation state of Mn in the compound is +3.

Figure 4 shows the charge-discharge curve and the corresponding dQ/dV plot, measured between 2.0 and 4.8 V at C/10 rate ($1C = 280 \text{ mA g}^{-1}$) at the 1st, 2nd, and 5th cycles. The cell exhibits two charging voltage plateaus at 3.45 and 4.3 V. The plateau at 4.5 V which is typical for the activation

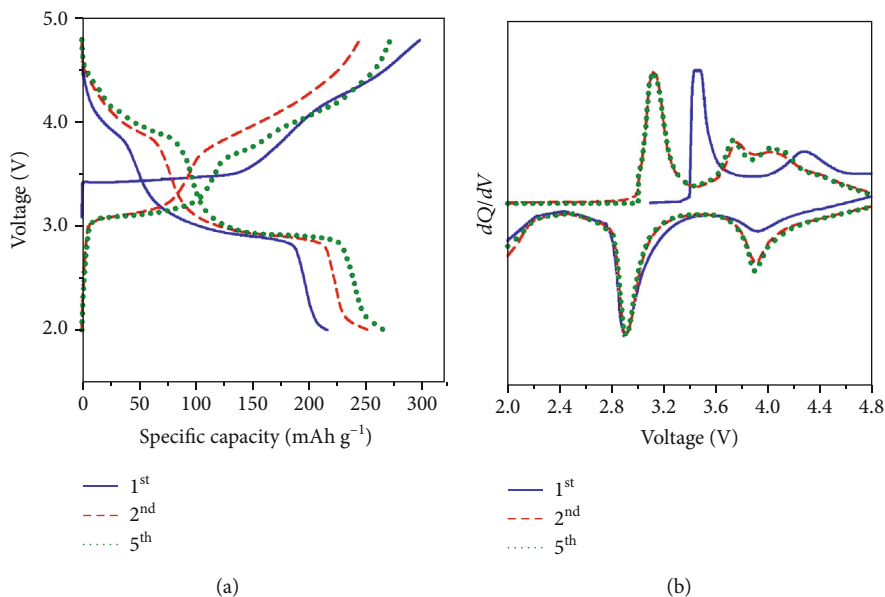


FIGURE 4: (a) Charge-discharge profiles and (b) corresponding dQ/dV plots for the 1st, 2nd, and 5th cycles of the sample.

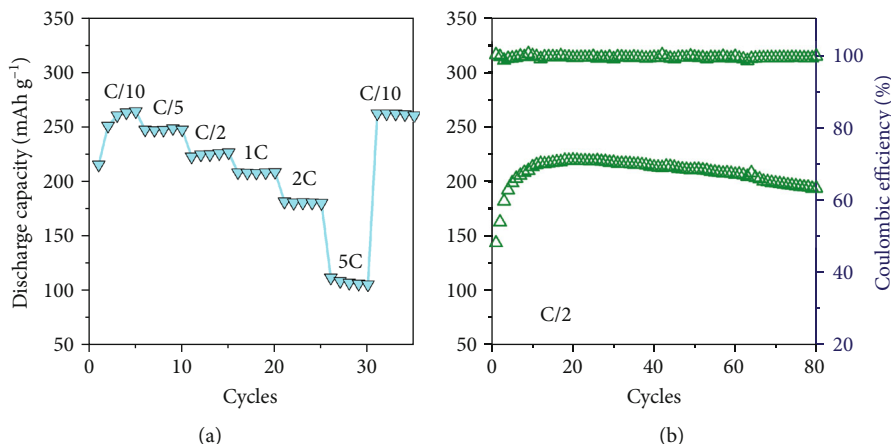


FIGURE 5: Cycling stability of the sample at (a) different C-rates and (b) at C/2.

of Li_2MnO_3 does not appear. It might be caused by the small fraction of the Li_2MnO_3 phase. The plateaus at 3.45 V are irreversible due to the structural change. For the first discharge, there is a plateau at 4 V and a long plateau ~ 3.0 V. The first charge and discharge capacity is 297 and 216 mAh g^{-1} , respectively. The low first Coulombic efficiency (72.7%) is due to the irreversible structural change during the first cycle of the LiMnO_2 and Li_2MnO_3 phase [4, 6, 25–31]. During cycling, the capacity contribution in the 4 V region increases, resulting in an increase in the overall capacity. After 5 cycles, the cathode could deliver a capacity of 265 mAh g^{-1} , which is higher than those reported in the literature [20, 32–37]. The dQ/dV plot (Figure 4(b)) shows peaks that correspond to the plateaus observed in Figure 4(a). For the first cycle, the peak at 3.5 V is irreversible while the peak at 4.3 V is reversible and there is a strong peak appearing at 2.9 V. For the subsequent cycles, the peak at 4.3 V shifts to lower voltage and induces two peaks at 3.8 and 4.0 V. These are typical peaks of spinel LiMnO_4 , indicating

the transformation of $o\text{-LiMnO}_2$ to a spinel-like phase during cycling [38].

A fresh cell was cycled 5 times at each C-rate including C/10, C/5, C/2, 1C, 2C, and 5C between 2.0 and 4.8 V to check its C-rate performance. Figure 5(a) shows the resulting discharge capacities. At C/10 rate, the highest capacity of 265 mAh g^{-1} is obtained after 5 cycles. With increasing C-rate, the capacities decrease as expected. The capacity is 249, 226, 208, 180, and 103 mAh g^{-1} for C/5, C/2, 1C, 2C, and 5C, respectively. The capacity is still as high as 263 mAh g^{-1} at C/10 after a severe test at 5C. Figure 5(b) shows the cycling stability and Coulombic efficiency of the sample at C/2. The capacity increases gradually over the first 12 cycles due to the transition of $o\text{-LiMnO}_2$ to a new spinel-like phase [4, 39]. However, the transformation is slow in this compound due to the stabilization of the Li_2MnO_3 phase. After 80 cycles, the capacity retention is 93%. The Coulombic efficiency is close to 100%, indicating less energy loss during the charge-discharge process.

4. Conclusion

o-LiMnO₂ was successfully synthesized by the hydrothermal method. The XRD and XPS results show the existence of the Li₂MnO₃ phase. SEM and TEM analyses confirmed the presence of a dominant *o*-LiMnO₂ phase with particle sizes in the range of 100–400 nm. The galvanostatic cycling demonstrates that a high capacity of 265 mAh g⁻¹ and 93% capacity retention after 80 cycles at C/2 could be achieved with this cathode. The structural change from the initial phase to the spinel-like phase is retarded due to the stabilization of the Li₂MnO₃ phase. Lastly, this work promotes environmentally friendly, low-cost, and high-capacity cathode materials for LIBs.

Data Availability

The data used to support the findings of this study are available from the corresponding author upon request.

Conflicts of Interest

The authors declare that there is no conflict of interest regarding the publication.

Acknowledgments

This research is funded by the Vietnam National Foundation for Science and Technology Development (NAFOSTED) under grant number 103.02-2019.26 and the Ministry of Science and Technology of Vietnam under the project code NĐT.75.CHN/19.

References

- [1] P. Yan, J. Zheng, J. Xiao, C.-M. Wang, and J.-G. Zhang, “Recent advances on the understanding of structural and composition evolution of LMR cathodes for Li-ion batteries,” *Frontiers in Energy Research*, vol. 3, no. 26, pp. 1–10, 2015.
- [2] Z. Yang, J. Zhang, M. C. W. Kintner-Meyer et al., “Electrochemical energy storage for green grid,” *Chemical Reviews*, vol. 111, no. 5, pp. 3577–3613, 2011.
- [3] B. Li, W. Zhao, C. Zhang et al., “Monodispersed LiFePO₄@C core-shell nanoparticles anchored on 3D carbon cloth for high-rate performance binder-free lithium ion battery cathode,” *Journal of Nanomaterials*, vol. 2020, Article ID 2607017, 11 pages, 2020.
- [4] Y. I. Jang, B. Huang, H. Wang, D. R. Sadoway, and Y. M. Chiang, “Electrochemical cycling-induced spinel formation in high-charge-capacity orthorhombic LiMnO₂,” *Journal of the Electrochemical Society*, vol. 146, no. 9, pp. 3217–3223, 1999.
- [5] D. Y. W. Yu and K. Yanagida, “Structural analysis of Li₂MnO₃ and related Li-Mn-O materials,” *Journal of the Electrochemical Society*, vol. 158, no. 9, pp. A1015–A1022, 2011.
- [6] D. Y. W. Yu, K. Yanagida, Y. Kato, and H. Nakamura, “Electrochemical activities in Li₂MnO₃,” *Journal of the Electrochemical Society*, vol. 156, no. 6, pp. A417–A424, 2009.
- [7] D. Kim, G. Sandi, J. R. Croy et al., “Composite ‘layered-layered-spinel’ cathode structures for lithium-ion batteries,” *Journal of the Electrochemical Society*, vol. 160, no. 1, pp. A31–A38, 2013.
- [8] J. C. Im, N. H. Vu, H. Tran Huu, D. S. H. Lee, and W. B. Im, “Effects of fluorine doping on electrochemical performance of spinel-layered Li₃Mn₃O_{7.5-x}F_x as cathode materials for Li-ion batteries,” *Journal of the Electrochemical Society*, vol. 166, no. 8, pp. A1568–A1573, 2019.
- [9] M. Freire, N. V. Kosova, C. Jordy et al., “A new active Li-Mn-O compound for high energy density Li-ion batteries,” *Nature Materials*, vol. 15, no. 2, pp. 173–177, 2016.
- [10] Y. Liu, G. Liu, H. Xu et al., “Low-temperature synthesized Li₄Mn₅O₁₂-like cathode with hybrid cation- and anion-redox capacities,” *Chemical Communications*, vol. 55, no. 56, pp. 8118–8121, 2019.
- [11] D. Y. Wan, Z. Y. Fan, Y. X. Dong et al., “Effect of metal (Mn, Ti) doping on NCA cathode materials for lithium ion batteries,” *Journal of Nanomaterials*, vol. 2018, Article ID 8082502, 9 pages, 2018.
- [12] N. H. Vu, P. Arunkumar, J. C. Im, and W. B. Im, “High capacity Li_{1.5}MnTiO_{4+δ} as thermally stable core-shell-driven cathode materials for lithium-ion batteries,” *Journal of Alloys and Compounds*, vol. 704, pp. 459–468, 2017.
- [13] N. H. Vu, J. C. Im, S. Unithrattil, and W. B. Im, “Synergic coating and doping effects of Ti-modified integrated layered-spinel Li_{1.2}Mn_{0.75}Ni_{0.25}O_{2+δ} as a high capacity and long lifetime cathode material for Li-ion batteries,” *Journal of Materials Chemistry A*, vol. 6, no. 5, pp. 2200–2211, 2018.
- [14] Y.-I. Jang, W. D. Moorehead, and Y.-M. Chiang, “Synthesis of the monoclinic and orthorhombic phases of LiMnO₂ in oxidizing atmosphere,” *Solid State Ionics*, vol. 149, no. 3–4, pp. 201–207, 2002.
- [15] X. Huang, Q. Zhang, H. Chang, J. Gan, H. Yue, and Y. Yang, “Hydrothermal synthesis of nanosized LiMnO₂-Li₂MnO₃ compounds and their electrochemical performances,” *Journal of The Electrochemical Society*, vol. 156, no. 3, p. A162, 2009.
- [16] N. H. Vu, P. Arunkumar, J. C. Im et al., “Effect of synthesis temperature on the structural defects of integrated spinel-layered Li_{1.2}Mn_{0.75}Ni_{0.25}O_{2+δ}: a strategy to develop high-capacity cathode materials for Li-ion batteries,” *Journal of Materials Chemistry A*, vol. 5, no. 30, pp. 15730–15742, 2017.
- [17] A. Boulineau, L. Croguennec, C. Delmas, and F. Weill, “Structure of Li₂MnO₃ with different degrees of defects,” *Solid State Ionics*, vol. 180, no. 40, pp. 1652–1659, 2010.
- [18] R. Wang, X. Li, L. Liu et al., “A disordered rock-salt Li-excess cathode material with high capacity and substantial oxygen redox activity: Li_{1.25}Nb_{0.25}Mn_{0.5}O₂,” *Electrochemistry Communications*, vol. 60, pp. 70–73, 2015.
- [19] N. H. Vu, S. Unithrattil, V. H. Hoang, S. Chun, and W. B. Im, “Template-engaged synthesis of spinel-layered Li_{1.5}MnTiO_{4+δ} nanorods as a cathode material for Li-ion batteries,” *Journal of Power Sources*, vol. 355, pp. 134–139, 2017.
- [20] S. Komaba, S.-T. Myung, N. Kumagai, T. Kanouchi, K. Oikawa, and T. Kamiyama, “Hydrothermal synthesis of high crystalline orthorhombic LiMnO₂ as a cathode material for Li-ion batteries,” *Solid State Ionics*, vol. 152–153, pp. 311–318, 2002.
- [21] N. H. Vu, H. T. T. Le, V. H. Hoang et al., “Highly N-doped, H-containing mesoporous carbon with modulated physicochemical properties as high-performance anode materials for Li-ion and Na-ion batteries,” *Journal of Alloys and Compounds*, vol. 851, article 156881, 2021.

- [22] Z. Zheng, W.-B. Hua, C. Yu et al., "Heterogeneous intergrowth $x\text{Li}_{1.5}\text{Ni}_{0.25}\text{Mn}_{0.75}\text{O}_{2.5-(1-x)}\text{Li}_{0.5}\text{Ni}_{0.25}\text{Mn}_{0.75}\text{O}_2$ ($0 \leq x \leq 1$) composites: synergistic effect on electrochemical performance," *Dalton Transactions*, vol. 44, no. 32, pp. 14255–14264, 2015.
- [23] J. Sicklinger, M. Metzger, H. Beyer, D. Pritzl, and H. A. Gasteiger, "Ambient storage derived surface contamination of NCM811 and NCM111: performance implications and mitigation strategies," *Journal of the Electrochemical Society*, vol. 166, no. 12, pp. A2322–A2335, 2019.
- [24] D. Briggs, G. E. Muilenberg, Perkin-Elmer Corp, "Handbook of X-ray Photoelectron Spectroscopy," in *Surface and Interface Analysis*, C. D. Wanger, W. M. Riggs, L. E. Davis, and J. F. Moulder, Eds., vol. 3, no. 4, pp. 78–79, Physical Electronics Division, Eden Prairie, Minnesota, USA, 1981.
- [25] Z. X. Shu, I. J. Davidson, R. S. McMillan, and J. J. Murray, "Electrochemistry of LiMnO_2 over an extended potential range," *Journal of Power Sources*, vol. 68, no. 2, pp. 618–622, 1997.
- [26] J. Lim, J. Moon, J. Gim et al., "Fully activated Li_2MnO_3 nanoparticles by oxidation reaction," *Journal of Materials Chemistry*, vol. 22, no. 23, pp. 11772–11777, 2012.
- [27] A. D. Robertson and P. G. Bruce, "Mechanism of electrochemical activity in Li_2MnO_3 ," *Chemistry of Materials*, vol. 15, no. 10, pp. 1984–1992, 2003.
- [28] R. Wang, X. He, L. He et al., "Atomic structure of Li_2MnO_3 after partial delithiation and re-lithiation," *Advanced Energy Materials*, vol. 3, no. 10, pp. 1358–1367, 2013.
- [29] D. Y. W. Yu, K. Yanagida, Y. Kato, and H. Nakamura, "Electrochemical activities in $\text{Li}_{[\text{sub } 2]} \text{MnO}_{[\text{sub } 3]}$," *Journal of the Electrochemical Society*, vol. 156, no. 6, pp. A417–A424, 2009.
- [30] N. H. Vu, V.-D. Dao, H. Tran Huu, and W. B. Im, "Effect of synthesis temperature on structure and electrochemical performance of spinel-layered $\text{Li}_{1.33}\text{MnTiO}_{4+z}$ in Li-ion batteries," *Energies*, vol. 13, no. 11, p. 2962, 2020.
- [31] N. H. Vu, V.-D. Dao, H. N. Van et al., "Spinel-layered $\text{Li}_2\text{MnTiO}_{4+z}$ nanofibers as cathode materials for Li-ion batteries," *Solid State Sciences*, vol. 103, article 106178, 2020.
- [32] S. T. Myung, S. Komaba, and N. Kumagai, "Synthesis of orthorhombic LiMnO_2 as a high capacity cathode for Li-ion battery by emulsion drying method," *Chemistry Letters*, vol. 30, no. 6, pp. 574–575, 2001.
- [33] X.-D. Li, W.-S. Yang, S.-C. Zhang, D. G. Evans, and X. Duan, "The synthesis and characterization of nanosized orthorhombic LiMnO_2 by in situ oxidation-ion exchange," *Solid State Ionics*, vol. 176, no. 7–8, pp. 803–811, 2005.
- [34] S.-h. Wu and M.-t. Yu, "Preparation and characterization of LiMnO_2 cathode materials," *Journal of Power Sources*, vol. 165, no. 2, pp. 660–665, 2007.
- [35] S. Chen, F. Cao, F. Liu et al., "Facile hydrothermal synthesis and electrochemical properties of orthorhombic LiMnO_2 cathode materials for rechargeable lithium batteries," *RSC Advances*, vol. 4, no. 26, pp. 13693–13703, 2014.
- [36] W. K. Pang, J. Y. Lee, Y. S. Wei, and S. H. Wu, "Preparation and characterization of Cr-doped LiMnO_2 cathode materials by Pechini's method for lithium ion batteries," *Materials Chemistry and Physics*, vol. 139, no. 1, pp. 241–246, 2013.
- [37] X. Xiao, L. Wang, D. Wang, X. He, Q. Peng, and Y. Li, "Hydrothermal synthesis of orthorhombic LiMnO_2 nano-particles and LiMnO_2 nanorods and comparison of their electrochemical performances," *Nano Research*, vol. 2, no. 12, pp. 923–930, 2009.
- [38] S.-T. Myung, S. Komaba, and N. Kumagai, "Hydrothermal synthesis and electrochemical behavior of orthorhombic LiMnO_2 ," *Electrochimica Acta*, vol. 47, no. 20, pp. 3287–3295, 2002.
- [39] R. J. Gummow, D. C. Liles, and M. M. Thackeray, "Lithium extraction from orthorhombic lithium manganese oxide and the phase transformation to spinel," *Materials Research Bulletin*, vol. 28, no. 12, pp. 1249–1256, 1993.